

# Use of Superlattice Structure To Control Reaction Mechanism: Kinetics and Energetics of Nb<sub>5</sub>Se<sub>4</sub> Formation

Masafumi Fukuto, Marc D. Hornbostel, and David C. Johnson\*

Contribution from the Department of Chemistry and Materials Science Institute, University of Oregon, Eugene, Oregon 97403

Received April 4, 1994\*

**Abstract:** This paper presents a study of the reaction of thin film niobium/selenium multilayers as a function of layer thickness. Diffraction and calorimetry data show a distinct difference in reactions between films with layer thicknesses above and below 60 Å. The thicker films are shown to nucleate Nb<sub>5</sub>Se<sub>4</sub> heterogeneously at the niobium-selenium interfaces. Thinner films form kinetically stable amorphous reaction intermediates before crystallizing Nb<sub>5</sub>Se<sub>4</sub> homogeneously. The nucleation barrier was measured using a Kissinger analysis demonstrating the kinetic stability of the amorphous intermediate. An energy versus reaction progress diagram is presented that contrasts the two reaction mechanisms.

## Introduction

Molecular chemistry is based upon the stepwise transformation of reactants to products, using kinetic control to optimize the yield of each intermediate product. These transformations are facilitated by reasonable reaction rates under mild reaction conditions. The kinetic barriers, rather than the true thermodynamic minimum of the system, control the reactions. The development of reagents which lower the kinetic barriers for specific reactions has permitted the rational design of intricate, multistep synthetic pathways. The design of these pathways is greatly aided by understanding the underlying reaction mechanisms which are used to predict the relationships between reaction conditions and product distributions.

A long-term goal of solid-state chemists has been to develop similar kinetic control in the synthesis of new compounds.<sup>1-3</sup> This has proven to be very difficult, however, due to the lack of information concerning the transformation of reactants (either solids or molecular precursors) to products.<sup>1,4</sup> While the principal phenomena occurring at a reacting interface (interdiffusion of the reactants, nucleation of crystalline compounds, and growth of these products) have been identified, the mechanisms of these phenomena are still not well understood on the atomic scale. Indeed, the typical last step in the formation of a solid-state compound, even from a molecular precursor, is simply an extended heating at elevated temperature during which the reactants rearrange to form the thermodynamic product. This high-temperature annealing is required to increase the diffusion rate, the limiting step in a typical solid-state reaction. The challenges in developing a synthetic route in which nucleation provides kinetic control are the following: to eliminate diffusion as a rate-limiting step, develop a basic understanding of the reaction energetics, and develop techniques to use reaction parameters, such as composition, to control the nucleation event.

Since interdiffusion, nucleation, and growth occur simultaneously at various rates depending upon the surfaces reacting in a heterogeneous system, understanding or controlling these reactions is a difficult task. Experimentally, solid-state reactions can be simplified by forming diffusion couples consisting of the reactants in direct contact with a specific crystallographic

orientation. For bulk diffusion couples, all thermodynamically stable compounds will eventually nucleate and grow. The thickness of each phase is determined by the diffusion rate of the reactants.<sup>5</sup> If films with layer thicknesses of a few hundred angstroms are made, one observes only one phase forming, which grows until it exhausts the supply of the limiting reactant. As the reaction proceeds, a second phase will nucleate at the remaining product-reactant interface and will grow until it exhausts the supply of either the remaining initial reactant or the first phase formed. This sequential evolution of phases continues until the final equilibrium mixture of compounds is formed. Some phases may not be formed, since those with large nucleation barriers will be skipped.<sup>6,7</sup> In both thick and thin diffusion couples, compounds are nucleated at the interface between two phases; the nucleation depends on the local composition gradients, stresses, and defects at the interface. In these heterogeneous systems, even basic chemical parameters such as overall composition cannot be used to control the nucleation process.

In the early 1980s, it was found that some metal-metal diffusion couples react to form a homogeneous amorphous metal alloy if the initial thicknesses of the two metals are less than a critical value.<sup>8-10</sup> These amorphous intermediates crystallize exothermically on annealing. This "ultrathin" film diffusion couple behavior has since been observed for a small number of systems, almost all of which are metal-metal or metal-silicon diffusion couples.<sup>11</sup> The critical thickness for the diffusion couple arises from the competition between diffusion and heterogeneous nucleation at the interfaces. Diffusion time scales as distance squared while to a first approximation interfacial nucleation should be independent of the thickness of the elements to either side of the interface. Thus, if the interfaces are made small enough, the elements will interdiffuse and the interfaces will disappear before nucleation can occur. The compound must then nucleate without the aid of stresses, strains, and composition gradients present at the interface.

While the above argument does not depend on the particular system, there is no guarantee that in a particular system the critical thickness and the nucleation energetics are such that the

(5) Brophy, J. H.; Rose, R. M.; Wulff, J. *The Structure and Properties of Materials*; John Wiley & Sons: New York, 1964; Vol. 2, pp 98-108.

(6) Bené, R. W. *Appl. Phys. Lett.* **1982**, *41*, 529-531.

(7) Walser, R. M.; Bené, R. W. *Appl. Phys. Lett.* **1976**, *28*, 624-625.

(8) Schwarz, R. B.; Johnson, W. L. *Phys. Rev. Lett.* **1983**, *51*, 415-418.

(9) Schwarz, R. B.; Wong, K. L.; Johnson, W. L. *J. Non-Cryst. Solids* **1984**, *61 & 62*, 129-134.

(10) Cotts, E. J.; Meng, W. J.; Johnson, W. L. *Phys. Rev. Lett.* **1986**, *57*, 2295-2298.

(11) Clemens, B. M.; Sinclair, R. *MRS Bull.* **1990**, 19-28.

\* To whom correspondence should be addressed.

• Abstract published in *Advance ACS Abstracts*, September 1, 1994.

(1) Stein, A.; Keller, S. W.; Mallouk, T. E. *Science* **1993**, *259*, 1558-1564.

(2) DiSalvo, F. J. In *Advancing Materials Research*; Psaras, P. A., Langford, H. D., Eds.; National Academy Press: Washington, DC, 1987; pp 161-176.

(3) DiSalvo, F. J. *Science* **1990**, *247*, 649-655.

(4) Schäfer, H. *Angew. Chem., Int. Ed. Engl.* **1971**, *10*, 43-50.

**Table 1.** Summary of Layer Thicknesses and Stoichiometry for the Samples Discussed<sup>a</sup>

sample number	total layer thickness (Å)	number of layers	stoichiometry	niobium layer thickness (Å)	selenium layer thickness (Å)
1	190	7	Nb <sub>5</sub> Se <sub>3,6</sub>	94	96
2	95	25	Nb <sub>5</sub> Se <sub>3,3</sub>	47	48
3	52	30	Nb <sub>5</sub> Se <sub>3,8</sub>	29	23
4	40	40	Nb <sub>5</sub> Se <sub>4,4</sub>	24	16
5	25	55	Nb <sub>5</sub> Se <sub>4,4</sub>	15	10
6	18	40	Nb <sub>5</sub> Se <sub>4,0</sub>	10	8

<sup>a</sup> The stoichiometry was determined by thermal-gravimetric analysis. The total layer thickness was determined by low-angle X-ray diffraction. The elemental layer thicknesses were determined from thickness calibration data as discussed in the text.

formation of an amorphous phase is feasible. Therefore, questions remain concerning the universality of this phenomena and the energetics of the transformations from the reactants to the amorphous state and from the amorphous state to the crystalline products. If it can be shown that this ultrathin film behavior is common to many binary and ternary systems, then the low-temperature annealing of thin multilayer films can be used as a general synthetic route to amorphous intermediates. This provides a solution to the first of the synthetic challenges mentioned above, as well as an opportunity to explore the use of nucleation to kinetically control final products.

This paper presents a detailed study of the thickness dependence of the reaction between niobium and selenium and the energetics of the ultrathin film reaction to form Nb<sub>5</sub>Se<sub>4</sub>. The niobium-selenium system was chosen for a number of reasons. It contains seven different compounds: Nb<sub>2</sub>Se, Nb<sub>3</sub>Se<sub>4</sub>, Nb<sub>3</sub>Se<sub>4</sub>, Nb<sub>2</sub>Se<sub>3</sub>, NbSe<sub>2</sub>, NbSe<sub>3</sub>, and Nb<sub>2</sub>Se<sub>9</sub>. Each of these compounds has a narrow composition range.<sup>12</sup> This permits the study of the extent to which the composition of the multilayer controls which of the many possible compounds crystallizes. In particular, the compound NbSe<sub>2</sub> is difficult to avoid in conventional, high-temperature synthesis presumably because it is the initial compound to nucleate at the reacting interfaces. These compounds have extended, covalently bonded structures. Specifically, Nb<sub>5</sub>Se<sub>4</sub> can be thought of as consisting of columns of apex-sharing niobium octahedra with selenium molecules in a square planar arrangement around each shared niobium. There is significant Nb-Nb and Nb-Se-Nb bonding between columns, forming a three-dimensionally connected network. This allows the ultrathin film behavior to be extended to systems containing complex, covalently bonded structures. For multilayer films with compositions near Nb<sub>5</sub>Se<sub>4</sub>, we show that we can prepare amorphous reaction intermediates in this system and use stoichiometry to control the nucleation of Nb<sub>5</sub>Se<sub>4</sub> from the amorphous reaction intermediate. The energetics of the reaction, including the kinetic barrier for the nucleation of Nb<sub>5</sub>Se<sub>4</sub>, are derived from experimental data. Finally, we discuss the application of this information to the design of a synthesis method for niobium- and selenium-containing ternary compounds.

## Experimental Procedures

**Sample Preparation.** A custom-built ultrahigh vacuum chamber<sup>13</sup> with independently-controlled deposition sources was used to prepare the multilayer films. Niobium was deposited at a rate of 0.8 Å/s using a Thermionic e-beam Gun source which was controlled by a Leybold-Inficon XTC quartz crystal thickness monitor. A Knudsen source was used to deposit selenium at a rate of 0.5 Å/s, as monitored by a separate quartz crystal monitor. Accumulation of an elemental layer was allowed to proceed until the thickness monitor reported that the desired layer thickness had been achieved (to the nearest angstrom). A shutter was then closed over the source, and the substrate was repositioned in preparation for deposition of the next elemental layer.

The multilayer films were simultaneously deposited on two adjacent substrates, one polished ( $\pm 3$  Å rms) silicon wafer and one poly-

(methylmethacrylate) (PMMA)-coated wafer.<sup>14</sup> The polished wafers were used for low-angle X-ray diffraction. The films on the PMMA-coated wafers were lifted off by immersing the wafers in acetone. The suspended samples were filtered and washed to remove dissolved PMMA and then collected and vacuum dried in aluminum DSC pans.

Thickness calibration of the deposition sources was done by preparing a series of samples with increasing thickness of one of the elemental components. The multilayer repeat distance was measured by low-angle X-ray diffraction. The thickness of each elemental layer was extracted from the variation of the total thickness with the intended thickness of each component. This calibration was done for layer thicknesses between 5 and 45 Å for niobium and 5 and 40 Å for selenium.

**Determination of Stoichiometry.** The thermal-gravimetric mass change of the samples on oxidation, resulting in the loss of selenium and the formation of Nb<sub>2</sub>O<sub>5</sub>, was used to determine stoichiometry. A calibration curve was constructed which allowed determination of layer thickness values required to obtain a given stoichiometry. Subsequent samples were prepared using this calibration curve, and the stoichiometry was checked for each sample by thermal-gravimetric analysis.

**X-ray Diffraction.** The low-angle diffraction resulting from the periodic layered structure of the as-deposited multilayer films was used to determine modulation thicknesses and interfacial widths.<sup>15-19</sup> These data were collected on a Scintag XDS 2000  $\theta$ - $\theta$  diffractometer with a sample stage modified to allow rapid and precise alignment.<sup>20,21</sup> High-angle diffraction data were used to determine whether the as-deposited, lifted, or subsequently annealed samples contained crystalline elements or compounds.

**Differential Scanning Calorimetry (DSC).** The evolution of the samples as they were subjected to elevated temperatures was monitored by DSC utilizing a TA Instruments TA9000 calorimeter fitted with a 910DSC cell. Approximately 1 mg of sample was used for each experiment. The sample was heated from ambient temperature to 550 °C at rates from 5 to 20 °C/min under flowing nitrogen and then allowed to cool back to room temperature. Without disturbing the sample or instrument in any way, this cycle was repeated two more times. The net heat flow associated with irreversible changes in the sample was found by subtracting the data for the third heating from those for the first. A measure of the repeatability of the experiment, and of the degree to which any irreversible changes had gone to completion during the first heating, was found by subtracting the data for the third heating from those for the second.

## Results and Discussion

Six samples were prepared with compositions near Nb<sub>5</sub>Se<sub>4</sub>. Table 1 summarizes the measured layer thicknesses and stoichiometries of these samples. The total layer thickness was determined from the position of the superlattice Bragg peaks in the low-angle X-ray diffraction data. The interfacial width was estimated from the d-spacing of the highest order observed Bragg

(14) Fister, L.; Johnson, D. C. *J. Am. Chem. Soc.* **1992**, *114*, 4639-4644.

(15) Xu, Z.; Tang, Z.; Kevan, S. D.; Novot, T.; Johnson, D. C. *J. Appl. Phys.* **1993**, *74*, 905-912.

(16) Barbee, T. W., Jr. *MRS Bull.* **1990**, *15*, 17.

(17) McWhan, D. B. In *Synthetic Modulated Structures*; Chang, L. C., Giessen, B. C., Eds.; Academic Press: New York, 1985; pp 43-74.

(18) Névot, L.; Pardo, B.; Corno, J. *Rev. Phys. Appl.* **1988**, *23*, 1675-1686.

(19) Spiller, E. In *Physics, Fabrication, and Applications of Multilayered Structures*; Dhez, P., Weisbuch, C., Eds.; Plenum Press: New York, 1988; Vol. 182, pp 271-309.

(20) Novot, T.; Fister, L.; Grant, C. A.; Johnson, D. C. In *Supramolecular Architecture: Synthetic Control in Thin Films and Solids*; Bein, T., Ed.; American Chemical Society: Washington, DC, 1992; Vol. 499; pp 355-368.

(21) Novot, T.; McConnell, J. M.; Johnson, D. C. *Chem. Mater.* **1992**, *4*, 473-478.

(12) *Binary Alloy Phase Diagrams*, 2nd ed.; Massalski, T. B., Okamoto, H., Subramanian, P. R., Kacprzak, L., Eds.; ASM International: Metals Park, OH, 1990; Vol. 3, pp 2664-2665.

(13) Fister, L.; Li, X.-M.; McConnell, J.; Novot, T.; Johnson, D. C. *J. Vac. Sci. Technol.* **1992**, in press.

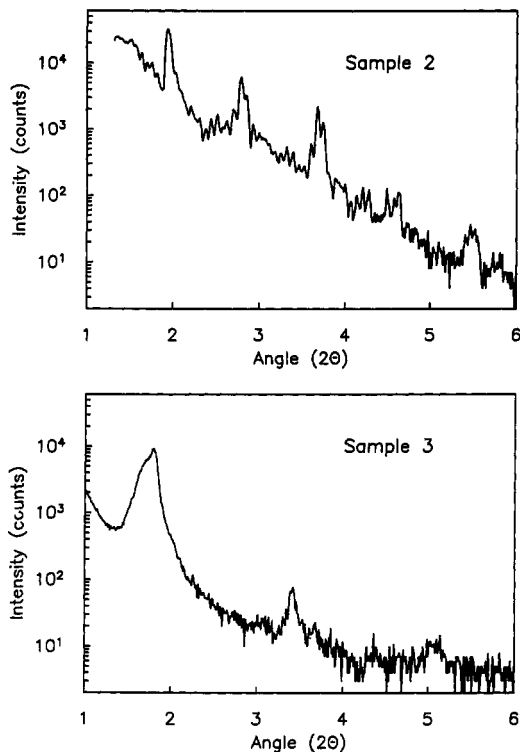


**Figure 1.** Representative low-angle diffraction data demonstrating the elemental modulation in the samples as deposited.

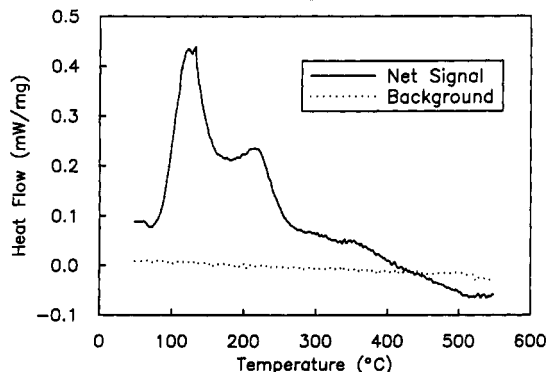


**Figure 2.** Differential scanning calorimetry data collected on sample 2 at a scanning rate of 10 deg/min.

peak. This peak corresponds to the highest frequency variation in the sample's composition profile and therefore provides a measured limit on the sharpness of the layer interfaces. This interfacial width is due to both interdiffusion of the elements and coherent roughness of the interfaces, which cannot be distinguished by X-ray diffraction. For all of these samples, the interfacial width is approximately 20 Å. In the thickest samples, crystalline niobium peaks were observed in high-angle X-ray data. In these samples, the layer thickness is large compared to the interfacial width and the composition profile varies from almost pure niobium to almost pure selenium. In the thinnest samples, the interfacial width is comparable to the layer thickness and only one superlattice Bragg peak is observed. This indicates that the composition modulation is sinusoidal, oscillating between niobium-rich and niobium-poor regions.

The solid-state reaction between the layers in the superlattice samples was followed with differential scanning calorimetry. The data obtained for sample 2 are representative of the data obtained for samples with layer thicknesses greater than 90 Å. The DSC data, shown in Figure 2, contain two exotherms with maximum heat flow at 125 and 200 °C. Diffraction data obtained as a function of temperature indicate that small Nb<sub>5</sub>Se<sub>4</sub> crystallites

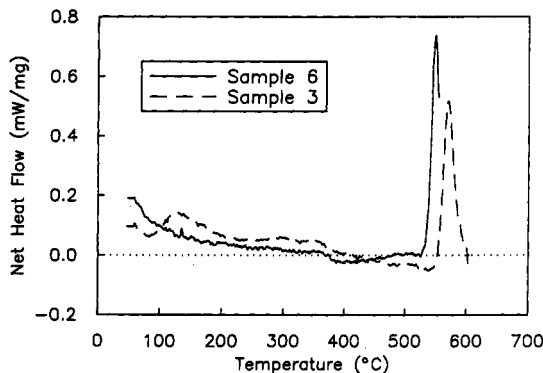


**Figure 3.** Differential scanning calorimetry data collected on samples 3 and 6 at a scanning rate of 10 deg/min.

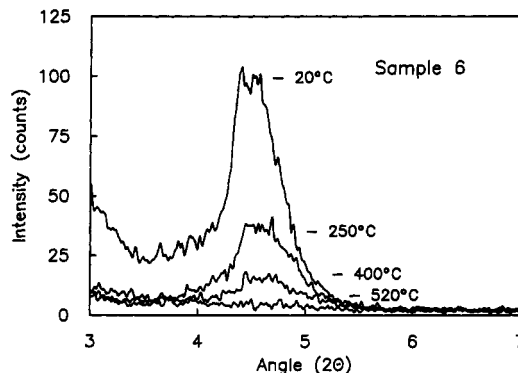


**Figure 4.** Decay of the first-order multilayer diffraction maxima as a function of annealing temperature for sample 6.

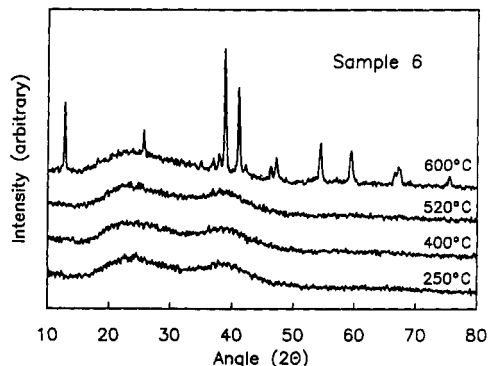


**Figure 5.** Evolution of the high-angle diffraction pattern as a function of annealing temperature for sample 6. The diffraction pattern after heating to 600 °C is that of Nb<sub>5</sub>Se<sub>4</sub>.

form after heating to 276 °C and that the sample remains compositionally modulated. Diffraction data collected after extended annealing at 600 °C indicate that the particle size of the crystallites reaches a limiting value consistent with the initial multilayer thickness. This behavior suggests that the Nb<sub>5</sub>Se<sub>4</sub> nucleates and grows out from the niobium-selenium interfaces.

Differential scanning calorimetry data obtained from samples 3 and 6, shown in Figure 3, are representative of the data obtained for samples with total layer thickness less than 60 Å. There are again two exotherms in these calorimetry traces: a broad low-temperature exotherm beginning at the initial heating and continuing to approximately 400 °C and a sharp exotherm between 550 and 600 °C. Figure 4 contains the low-angle diffraction data and Figure 5 contains the high-angle diffraction data collected on sample 6 after annealing to various temperatures. During annealing, the low-angle Bragg peaks decay steadily as the elemental modulation within the superlattice diffuses away. The decay of the low-angle Bragg diffraction peaks correlates with the broad low-temperature exotherm found in the DSC data.

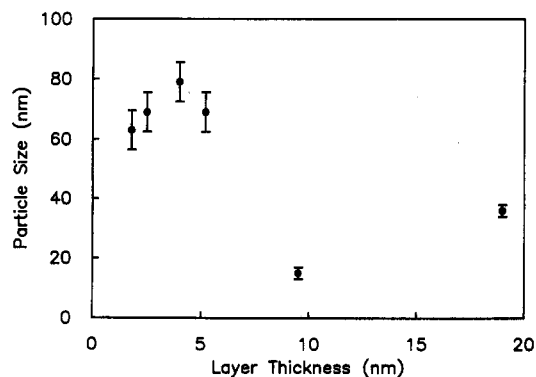


**Figure 6.** Calculated Nb<sub>5</sub>Se<sub>4</sub> particle sizes, using the Scherrer equation and X-ray diffraction line widths, versus total layer thickness. Errors are estimated from the variation of calculated sizes using the three most intense diffraction maxima.

The heat evolved in this exotherm represents a portion of the heat of mixing of niobium and selenium. After annealing at 520 °C, heat flow ceases and the low-angle diffraction peaks due to compositional modulation are no longer observed. High-angle X-ray diffraction indicates that the sample remains X-ray amorphous, even with continued annealing below 500 °C. Therefore, we have successfully prepared an homogeneous, amorphous intermediate phase. Heating the sample to 600 °C results in a sharp exotherm, and high-angle X-ray diffraction correlates this exotherm with the crystallization of Nb<sub>5</sub>Se<sub>4</sub>. The diffraction line widths of the crystalline Nb<sub>5</sub>Se<sub>4</sub> formed in this manner are considerably narrower than the line widths of samples formed from thicker multilayers, indicating significantly larger particle sizes. This is consistent with a high-temperature, homogeneous nucleation and subsequent growth of Nb<sub>5</sub>Se<sub>4</sub>. The large difference in the resultant particle size for the homogeneously and heterogeneously nucleated samples provides a clear demarcation between the two reaction pathways (see Figure 6).

The stability of the amorphous reaction intermediate was studied by collecting differential scanning calorimetry data as a function of scan rate to estimate the activation energy of the nucleation and growth process. Such non-isothermal DSC data are typically analyzed using a Kissinger analysis<sup>22</sup> in which the activation energy can be obtained from the peak temperature,  $T_p$ , as a function of scan rate,  $Q$ :

$$\frac{d \ln \left[ \frac{Q}{T_p^2} \right]}{d \left[ \frac{1}{T_p} \right]} = \frac{-E_{\text{crystallization}}}{R}$$

Graphing  $\ln[Q/T_p^2]$  versus  $1/T_p$ , as shown in Figure 7 for sample 4, gives a straight line with slope  $-E/R$  yielding a value of 2.7 eV for the activation energy. While this activation energy is associated with the nucleation and growth of Nb<sub>5</sub>Se<sub>4</sub>, its extraction from the non-isothermal DSC data is based upon many assumptions. The above equation is derived by assuming that the nucleation and growth can be described by the Johnson-Mehl-Avrami equation, that the amorphous and the crystalline states have the same composition, and that the nucleation and growth rates are constant at constant temperature. A further approximation is made that both the nucleation rate and growth rates may be described by Arrhenius expressions over the range of temperature in which the peak temperature varies with scan rate.

The thick and thin film reactions can be summarized with a free energy diagram, given in Figure 8. The energy levels shown, including the activation barrier to crystallization, are scaled according to the measured enthalpy data, given in the figure

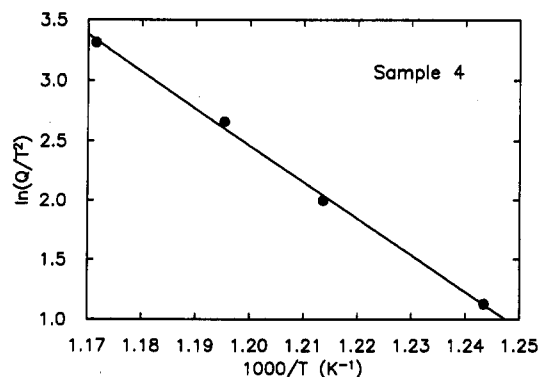


**Figure 7.** Kissinger plot for sample 4 used to derive the activation energy for nucleation of Nb<sub>5</sub>Se<sub>4</sub>. The arguments of the logarithm were made unitless by dividing by a constant,  $T_0^2/Q_0$ , where  $T_0$  is 1000 K and  $Q_0$  is 1 deg/min.

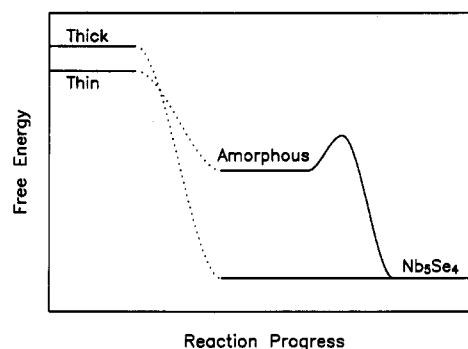


**Figure 8.** Schematic of the free energy of a sample as a function of reaction progress for thick and thin film samples illustrating the activation energy necessary to nucleate crystalline Nb<sub>5</sub>Se<sub>4</sub> from the amorphous reaction intermediate. The thick samples evolved approximately 140 kJ/mol during the heterogeneous nucleation and growth of Nb<sub>5</sub>Se<sub>4</sub>. The thin samples evolved approximately 60 kJ/mol as the elements interdiffused and 65 kJ/mol during crystallization.

caption. However, this is an idealized picture which is intended to contrast the two reaction types and should not be interpreted as an actual measurement of free energy as a function of time. Entropy effects have not been included, but such effects are usually small in solid-state reactions. For example, the entropy change in crystallizing the amorphous phase will be similar to that in crystallizing a liquid. Such entropy changes are typically on the order of 1 cal/(mol·K), which would correspond to less than 1% of the observed free energy change. Neglecting the entropy of mixing of the initial multilayers is expected to be the greatest source of error from excluding entropy effects. If this were included, the relative free energy of the multilayers would be greater and the thick and thin multilayers would have a greater separation than shown. However, the important features of Figure 8 would be unchanged.

Figure 8 illustrates how the free energies of multilayer composites vary as they evolve, contrasting the evolution of thick and thin multilayer composites. The thin multilayers start at a lower free energy than the thick because a greater fraction of the thin multilayer is within the 20 Å thick interface region. The thick multilayer samples interdiffuse and heterogeneously nucleate Nb<sub>5</sub>Se<sub>4</sub> at the interfaces at low temperatures, resulting in a drop in free energy from the reactants immediately to the products. The thin multilayer samples, however, evolve to an amorphous intermediate which is kinetically stable with respect to nucleation. The nucleation barrier is considerable, being approximately 25 kJ/mol of Nb<sub>5</sub>Se<sub>4</sub> nuclei, if we assume a critical nuclei size of approximately 7 Å in radius containing 10 Nb<sub>5</sub>Se<sub>4</sub> formula units. This large activation barrier is the reason the amorphous reaction intermediate is stable even after extended annealing at 500 °C. At higher temperatures the sample nucleates homogeneously.

Figure 8 illustrates the two main advantages of using interdiffusion of thin elemental layers in the synthesis of new compounds. The first is the ability to keep the sample in a high-energy state by preventing the heterogeneous formation of stable binary compounds. The second advantage is that the energetics of the nucleation process control the compound eventually formed, giving kinetic control. In principle, the ability to form a high-energy metastable intermediate allows the synthesis of compounds which are inaccessible by traditional approaches. A synthetically important example would be the preparation of ternary compounds which are unstable relative to disproportionation into binary components. The ability to prepare such compounds will depend upon controlling nucleation energetics such that the compound with the desired composition and structure nucleates preferentially. While composition of the amorphous reaction intermediate has been used to control nucleation, other techniques, such as seeding the composite with isostructural compounds, need to be developed. Further studies are required to explore how the activation energy for nucleation varies with composition and whether the activation energy is modified by seeding or epitaxial nucleation.

## Conclusion

The reaction between niobium and selenium multilayers as a function of layer thickness has been studied. A critical thickness was found, above which samples nucleate heterogeneously at interfaces and below which samples form a homogenous, kinetically stable reaction intermediate. The activation energy for the crystallization of this reaction intermediate was determined, permitting the construction of a free energy diagram for the reaction. The ability to form such a kinetically stable reaction intermediate and control its nucleation is the first step in developing a reaction route for solid-state reactions which is similar in philosophy to that used by molecular chemists. Before solid-state chemists can design a method using this kinetically controlled route to form solid-state compounds with desired structures, techniques to control nucleation energetics need to be developed.

**Acknowledgment.** This work was supported by the National Science Foundation (DMR-8704652 and DMR-9213352). Support by the Office of Naval Research (N0014-91-J-1288) and (N0014-93-1-0205) is gratefully acknowledged.